Experimental Tests of Entanglement Models of Rubber Elasticity. 2. Swelling

Moshe Gottlieb*

Chemical Engineering Department, Ben Gurion University of the Negev, Beer Sheva 84105, Israel

Richard J. Gaylord

Department of Metallurgy and Mining Engineering, University of Illinois at Urbana-Champaign, Urbana, Illinois 61801. *Received September 29, 1983*

ABSTRACT: Experimental swelling data are used to compare theoretical models of rubber elasticity. Of the nine models that were examined, only the Gaylord and Marrucci tube models, the modified Graessley primitive path model, and the Flory–Erman constrained junction fluctuation model provide even qualitative agreement with the observed network behavior. Quantitative agreement is impossible for the Flory–Erman model and requires physically unrealistic parameter values for the other three models. The assumed separability of elastic and mixing free energy terms remains questionable.

Introduction

A number of theoretical models have been proposed during the past few years to describe the entanglement contribution to cross-linked polymer network behavior. We have undertaken to compare the ability of these models to match experimental data for a variety of deformation conditions. In the first paper of this series,[1] uniaxial extension–compression behavior was examined. In this work, swelling behavior is considered.

It follows from the Flory–Rehner[2] assumption of the additivity of elastic and mixing free energies that, at equal solvent concentrations, the ratio of the solvent activity in a polymer when it is cross-linked ($a_{1,c}$) to the solvent activity in the same polymer when it is un-cross-linked ($a_{1,u}$) represents the elastic contribution to solvent activity. In a series of experiments conducted by Gee, Herbert, and Roberts[3] and by Eichinger and co-workers,[4-6] data were obtained for several polymer–solvent pairs for both bulk- and solution-cured networks. In every case, a pronounced maximum is exhibited in a plot of the dilation "modulus" $S = \lambda \ln (a_{1,c}/a_{1,u})$ against the deformation ratio λ, defined as $(v_2^0/v_2)^{1/3}$, where v_2 and v_2^0 are the polymer volume fractions in the swollen network and in the curing stage, respectively. Therefore, the ability to predict such a maximum must be considered a prerequisite for any theoretical model. It will be shown below that only a very limited number of the proposed models demonstrate even qualitatively the observed network swelling behavior.

Theoretical Models

The theoretical treatments of entanglement effects in cross-linked polymer networks can be roughly grouped into four categories:

1. Sliplink Models. Here, the network chain threads its way through a specific number of discrete small rings which represent the entanglement points. In the Marrucci version of the model,[7] the portions of the chain between consecutive sliplinks are taken to be able to adjust or equilibrate themselves by sliding freely through the sliplink so as to result in the same tension in each subchain. This version is therefore a direct offshoot of the Doi–Edwards model of the viscoelasticity of polymer liquids from which it is obtained by simply suppressing chain end retraction during the equilibration process. In the Ball–Doi–Edwards–Warner version of the model,[8] there is in addition to a parameter α, which measures the ratio of sliplinks to chemical junctions, a parameter η, which measures the ability of a sliplink to "slide" along the chain passing through it (η equal to zero corresponds to the phantom network model discussed below).

2. Junction Fluctuation Models. The earliest models of this type[9,10] assume that the fluctuations of network junctions about their mean positions are strain-independent. In one case,[9] called the affine network model, the flucutations are totally prohibited. In another case,[10] called the phantom network model, the fluctuations are completely uninhibited. In a recent, more sophisticated approach, called the constrained junction fluctuation model,[11,12] the fluctuations are taken to be strain-dependent, due to the profusion of diffuse, nonspecific entanglements. As a result, the fluctuations are suppressed at small strains and are free at large strains. This strain-dependent junction fluctuation effect has been modeled[12] by subjecting each junction to a domain of constraint. There are two parameters in the model: κ describing the severity of the entanglement constraints, and ζ measuring the departure from affine deformation of the a priori probability function for junction displacement.

3. Primitive Path Models. In these treatments, the segments of the network chain are divided into two distinct groups; the segments belonging to the "path" population lie along the primitive path, which is defined as the shortest path between chain ends that does not violate any topological constraints on the chain, and the remaining segments, which belong to the "excess" or "surplus" population and make local loops or side excursions from the primitive path without enclosing any obstacles. In deformation, the primitive path lengthens, which requires a transfer of segments from the "surplus" to the "path" population. In the Graessley version,[13] the transfer produces free energy changes due to the reduction in the number of surplus segments and the alteration in the distribution of orientations of path segments. The model has two parameters: a structural parameter $\alpha = N\nu/\xi$, N being the mean number of primitive path steps in a strand, ν the number of strands in the network, and ξ the cycle rank, and a topological parameter p representing the fraction of segments residing in the surplus population. When $p = {}^1/_3$, the model reduces to the Marrucci sliplink model. In the Edwards[14] "potential pipe" model, the transfer of segments causes a free energy change due to the remaining "surplus" population, which executes a random walk having one dimension along the primitive path and two dimensions that are orthogonal to the path and subject to a strain-invariant confining harmonic potential. The model has two parameters: β, which is proportional to the strength of the harmonic potential, and α, which represents the ratio of the primitive path length to the chain contour length.

0024-9297/84/2217-2024$01.50/0

4. Tube Models. This approach spatially restricts the entire network chain. This restriction is modeled either by assuming[15] that a harmonic potential of strength s acts on the chain segments in the direction lateral to the end-to-end chain separation or by assuming[16] that the chain is confined within a tube having its central axis along the end-to-end chain separation and a cross-sectional area a^2. The "soft" tube and "hard" tube are made equivalent[17] by setting $a^2 = s^{-1}$ in the limit of a long chain and small a and large s. For the entire network, it is assumed either that these tubes encompass chains which are randomly oriented[14,18] or that these tubes encompass the chains of the three-chain network model.[16,19] Both tube models[18,19] have looked at two possible tube deformation mechanisms that preserve the tube volume: the tube dimensions vary affinely, and the tube length deforms affinely while the tube cross section remains regular as its area varies inversely with the tube length.

The Marrucci random tube model has the two parameters l_0/a_0, which is the ratio of the tube length to the tube radius in the parent un-cross-linked polymer and r, which is the ratio of tube cross-sectional area before and after curing. Network imperfections and unreacted polymeric material have a diluting effect, which tends to increase the tube radius; hence, $r = 1$ for a perfect network and $r < 1$ otherwise. Two cases have been considered by Marrucci[18]: (I) all network chains are long so that $ns \gg 1$ (n is the number of chain segments); (II) chains are distributed in size, with short chains ($ns < 1$) behaving as "phantom" network strands and long chains ($ns > 1$) behaving as in model I. The contribution of junctions or chain ends to the free energy of the network is ignored in model II.

The Gaylord three-tube model has two parameters: the quantities sl_0^2/nb^2 and nb^2r/a_0^2, where r, l_0, and a_0 have the same meaning as in the Marrucci model, s is the ratio of the tube length before and after curing, n is the number of segments in the chain, and b is the segment length.

Experimental Data

Four sets of data on solvent activity in cross-linked networks were used: (1) natural rubber swollen in benzene[3] at 25 °C; (2) poly(dimethylsiloxane) (PDMS) in benzene[6] at 30 °C; (3) PDMS in cyclohexane[6] at 30 °C; and (4) solution-cured PDMS in cyclohexane[5] at 30 °C (volume fraction of polymer at curing v_2^0 = 0.457).

The first three systems were bulk-cured while the last system was solution-cured. The networks were cross-linked either by γ radiation (PDMS) or by chemical reaction with dicumyl peroxide (natural rubber). In no case were there details on the network structure (e.g., the number of junctions, the average junction functionality, and the molecular weight between junctions), and therefore it was assumed that all of the systems were perfect, tetrafunctional networks; i.e., $\nu/2 = \mu = \xi$, where ν, μ, and ξ are the number of strands, the number of junctions, and the network cycle rank, respectively.

The actual experiments[3,4] consisted of taking differential mass measurements of the solvent uptake by the cross-linked network and by its un-cross-linked parent polymer under isopiestic conditions. These results were then converted into the ratio of the chemical activities of the solvent in the cross-linked and un-cross-linked systems at the same polymer volume fraction. To accomplish this conversion, the absolute solvent activity (vapor pressure) in either the cross-linked[3] or un-cross-linked[4-6] polymer had to be obtained, and volume additivity had to be assumed.

The smoothed experimental results were plotted in the form of the normalized dilation modulus S/S_0 against λ^2, where S is the dilation modulus and S_0 is its extrapolated value at $\lambda = 1$ (cf. Figures 6–9). The far ends of the experimental curves represent saturation points. The accuracy of the data varied from one system to another and also depended on the difference between solvent activity and unity (for further details, the reader is referred to the original papers[3-6]).

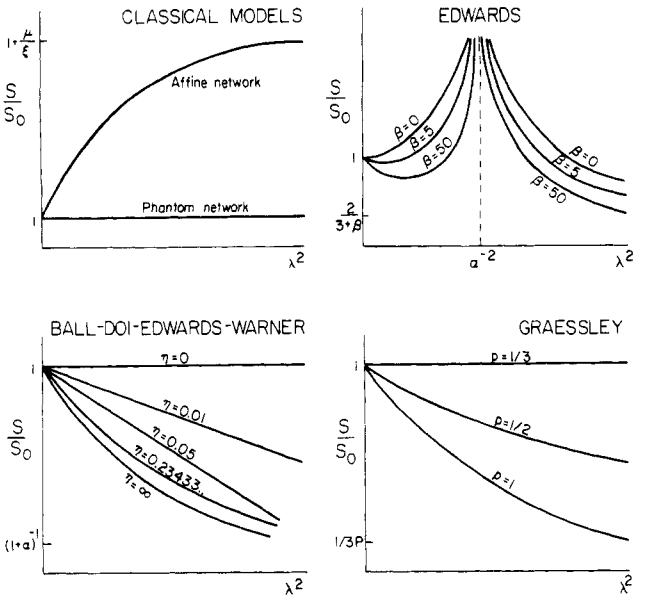

Figure 1. Schematic representation of the variation of the reduced dilation modulus with λ^2 for five different models: phantom network, affine network, Edwards primitive path tube model, the Ball–Doi–Edwards–Warner sliplink model, and the Graessley primitive path model.

The most salient feature in all of these data plots is the presence of a prominent maximum. Both its position and magnitude depend upon the solvent, the polymer, and the curing conditions. While some inaccuracy may have resulted from the difficulties in exactly determining S_0, this only affected the magnitude of the maxima, not their locations. The experimental maxima and saturation point data are summarized in Table I.

Testing Procedure

The predicted expressions for the reduced dilation modulus S/S_0 of nine models obtained by the procedure outlined in Appendix A are listed in Table II. Five of these are sketched in Figure 1. Any molecular model, in order to be acceptable, must at least predict a maximum in S/S_0. None of the models depicted in Figure 1 satisfies this necessary criterion and so can be eliminated from further discussion, with just a few comments on the details of the curves:

Phantom Network Model.[10] S/S_0 is independent of dilation, recalling a similar behavior of this model in uniaxial extension Mooney plots.

Affine Network Model.[9] S/S_0 monotonically approaches $1 + \mu/\xi$ at large dilation.

Ball–Doi–Edwards–Warner Sliplink Model.[8] S/S_0 monotonically decreases toward $1/(1 + \alpha)$ at large dilation when $\eta > 0$. When $\eta = 0$, phantom network behavior is recovered.

Edwards Potential Pipe Model.[14] Two modes of behavior occur. For $\alpha > 0$, the curves diverge at $\lambda^2 = 1/\alpha^2$, and S/S_0 has a limiting value of $2/(3 + \beta)$ at large dilation. When the parameter $\alpha = 0$, a family of curves similar to those shown for the BDEW model is obtained, with β determining their exact shape and with S/S_0 monotonically approaching a limiting value of $3/(3 + \beta)$ at large dilation. When both β and α equal zero, phantom network behavior is shown.

Graessley Primitive Path Model.[13] It is assumed that the entanglement contribution to network behavior is strictly additive to a phantom network term stemming from the contribution of the chemical network. For p not equal to $^1/_3$ and large N, S/S_0 monotonically approaches $1/3p$ at large dilation. When $p = {}^1/_3$, phantom network behavior occurs.

Table I
Summary of Experimental Data

system	$S_0 \times 10^2$	λ_{max}^2	$(S/S_0)_{max}$	λ_{satd}^2	$(S/S_0)_{satd}$	curing method
PDMS + benzene[6]	1.75	1.27	2.074	2.575	0.246	irradiation, bulk
PDMS + cyclohexane[6]	1.56	1.12	1.655	3.451	0.365	irradiation, bulk
PDMS + cyclohexane[5]	1.62	0.725	1.388	2.021	0.235	irradiation, solution
				0.593[a]	0.914[a]	
natural rubber + benzene[3]	2.74	1.81	1.337	2.21	1.004	chemical, bulk

[a] λ^2 and S/S_0 values for dry network. Network was solution-cured at $v_2^0 = 0.457$.

Table II
Reduced Dilation Modulus Expressions for the Models

model	S/S_0	parameters	remarks
phantom[10]	1		
affine[9]	$1 + (1 - \lambda^{-2})(\mu/\xi)$		$\mu/\xi = 1$ has been assumed
Edwards[14]	$\frac{2\lambda + \beta}{\lambda(3 + \beta)} + \left[\frac{1 - \alpha}{1 - \alpha\lambda} + \frac{\alpha\lambda(1 - \alpha)}{2(1 - \alpha\lambda)^2} - \frac{\alpha}{2\lambda(1 - \alpha\lambda)}\right](3 + \beta)^{-1}$	α, β	$\alpha = \beta = 0$ phantom network
Ball-Doi-Edwards-Warner[8]	$\frac{1}{1 + \alpha} + \frac{\alpha}{1 + \alpha}\frac{1 + 2\eta + \eta^2\lambda^2}{(1 + \eta\lambda^2)^2}$	$\alpha = N_s/\mu$ η	authors suggest $\eta = 0.23433\ldots$ $\eta = 0$ phantom network
Graessley[13]	$\left[1 + \alpha\frac{3p + \lambda - 1}{3p\lambda}\right]/(1 + \alpha)$	$\alpha = N\nu/\xi, p$	
modified Graessley	$\left[2 - \lambda^{-2} + \alpha\frac{3p + \lambda - 1}{3p\lambda}\right]/(1 + \alpha)$	α, p	
Marrucci I[18]	$(A - B\lambda^{-4} + \lambda^{-2})/(A - B + 1)$	A, B	$A = 2\frac{l_0\nu}{a_0\xi}$, $B = Ar$ (eq 38, ref 18)
Gaylord[19]			$A = \frac{3l_0^2 s\nu}{nb^2\xi}$, $B = \frac{2\pi^2 nb^2\nu}{3a_0^2\xi}r$
Marrucci II	$\beta^{-1}\{3/2 + \exp(-\alpha\lambda^2)[(\lambda^2/r - \lambda^{-2} - 3/2) + \alpha(3\lambda^2/2 - \lambda^4/r - 1) + \alpha^{-1}(1/r - \lambda^{-4})]\}$ $\beta = 3/2 + \exp(-\alpha)[(1/r - 5/2) + \alpha(1/2 - 1/r) + \alpha^{-1}(1/r - 1)]$	$r, l_0/a_0$	$\alpha = (rl_0/a_0)^{-1}$ (eq 73, ref 18)
Flory-Erman[12]	$1 + K(\lambda^2)$; $K(\lambda^2) = \frac{B}{1 + B}\frac{\partial B}{\partial(\lambda^2)} + \frac{Bg}{1 + Bg}\frac{\partial(Bg)}{\partial(\lambda^2)}$ $g = \lambda^2[\kappa^{-1} + \xi(\lambda - 1)]$; $B = (\lambda - 1)(1 + \lambda - \xi\lambda^2)(1 + g)^{-2}$	κ, ξ	

Table III
Model Parameter Values Used To Fit Data

system	Marrucci I–Gaylord		Marrucci II		modified Graessley		Flory–Erman	
	A	B	r	l_0/a_0	p	$N\nu/\xi$	κ	ζ
PDMS + benzene	−0.388	0.635	0.65	−3.3	0.119	−0.988	100	0.57
PDMS + cyclohexane	−0.430	0.560	0.41	−5.9	0.115	−1.00	100	1.15
solution-cured PDMS + cyclohexane	−0.503	0.362	0.13	−15.4	0.094	−0.922	1.9	2.7
			0.0046	52.1				
natural rubber + benzene	0.433	0.905	0.39	−16.9	0.117	−0.804	100	0.115
			0.40	10.8			1.3	8.35

For the remaining four models, several data-fitting schemes were tested. A nonlinear least-squares approach was ruled out since it usually resulted in a relatively flat curve having approximately half the observed maximum value of S/S_0. All the other schemes forced the models to pass through specific experimental points, such as the maximum or the saturation point. The data-fitting scheme presented here consisted of requiring a model to predict a maximum at the observed experimental λ_{max}^2. A second requirement (if it was attainable by the model under consideration) was that the model approximately match the experimental value of $(S/S_0)_{max}$, bearing in mind that a 10–20% error in this quantity may have been introduced due to difficulties in measuring activity differences at low solvent concentrations.

Modified Graessley Model. A straightforward modification of the original Graessley primitive path model is to assume that the permanent cross-links follow affine network behavior rather than phantom network behavior. The resulting mathematical expression for S/S_0 is given in Table II and has a maximum at

$$\lambda_{max} = 6p/[\alpha(3p - 1)] \tag{1}$$

Appropriate selection of the parameters p and α (which retain the same physical interpretation as in the original Graessley model) then enables us to match the experimentally observed maxima:

$$\alpha = \frac{2 - 2/\lambda_{max} + \lambda_{max}^{-2} - (S/S_0)_{max}}{(S/S_0)_{max} - 1} \tag{2}$$

$$p = \alpha\lambda_{max}/[3(\alpha\lambda_{max} - 2)] \tag{3}$$

Marrucci I and Gaylord Tube Models.[18,19] While, in general, the deformation expressions predicted by these two models are different (cf. ref 1), both models yield the same S/S_0 expression (differing only in their contants), which is shown in Table II. The quantity B, defined in Table II, is given by the maximum position:

$$\lambda_{max}^2 = 2B \tag{4}$$

The quantity A, defined in Table II, is then determined by the magnitude of the maximum:

$$A = \frac{(4B)^{-1} - (S/S_0)_{max}(1 - B)}{(S/S_0)_{max} - 1} \tag{5}$$

Marrucci II Model.[18] To obtain the two parameters for this version of Marrucci's model, the equation in Table II was solved with the appropriate λ_{max}^2 and $(S/S_0)_{max}$ values inserted for λ^2 and S/S_0, respectively. A second equation was obtained from the maximum criterion, resulting in the following expression:

$$\frac{\alpha^3}{r}(\lambda_{max}^2)^5 - \left(\frac{3}{2}\alpha^3 + \frac{3}{r}\alpha^2\right)(\lambda_{max}^2)^4 + (\alpha^3 + 3\alpha^2)(\lambda_{max}^2)^3 + \alpha^2(\lambda_{max}^2)^2 + 2\alpha(\lambda_{max}^2) + 2 = 0 \tag{6}$$

These two nonlinear equations were solved simultaneously for r and $\alpha = (rl_0/a_0)^{-1}$ by the successive overrelaxation method.

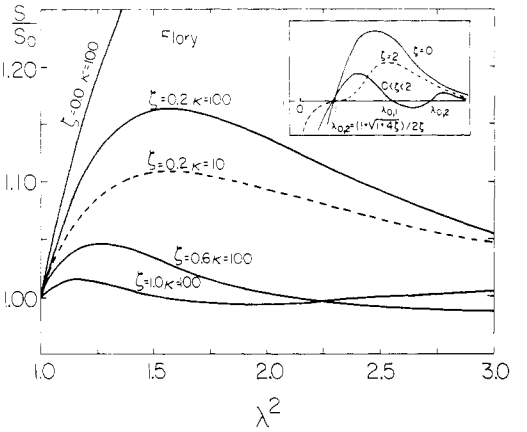

Figure 2. Calculated reduced dilation modulus for different values of the Flory–Erman model.

Flory–Erman Model.[12] The most recent form of the constrainted junction fluctuation model yields an S/S_0 expression, given in Table II, that is an extremely nonlinear function of λ^2. Both the magnitude and position of the predicted maxima depend strongly on *both* of the model parameters κ and ζ (contradicting the suggestion that ζ plays only a minor role[20]). This is shown in Figure 2. The inset in Figure 2 shows a schematic description of the dilation modulus function. For $\zeta = 0$ only one maximum is exhibited. Its location is always at $\lambda > 1$ and is determined by the value of κ. For $0 < \zeta < 2$ there are two maxima and one miminum, all of them at $\lambda > 1$. As ζ increases, the peak on the right increases whereas the peak on the left decreases until it entirely disappears for $\zeta = 2$. At the same time the peak positions are shifted leftward toward $\lambda = 1$. For $\zeta > 2$ (not shown) one peak and one minimum are located at $\lambda < 1$ and one maximum is located at $\lambda > 1$. Also, for certain combinations of κ and ζ (>2), $B = -1$ and the function is then undefined. As $\lambda \to \infty$, irrespective of ζ and κ, S/S_0 approaches the phantom network value of 1. In order to fit the model to the data, a relationship between the position and magnitude of the maximum (the one closest to $\lambda = 1$) and the two parameters is needed. Since we were unable to obtain a closed-form analytical expression of this sort, it was necessary to generate a set of graphical relations. This was done with Figures 3–5. First, sets of ζ,κ values were chosen from Figure 3 which show a maximum at the correct position. Next, using Figures 4 and 5, the final values were chosen so that the magnitude of the maximum $(1 + K)$ was close to the experimental values.

Results and Discussion

Table III indicates the values of the parameters that were found to best fit the various data sets for the different theoretical models. In Figures 6–9, the predicted theoretical curves are indicated by the dotted line (Flory–Er-

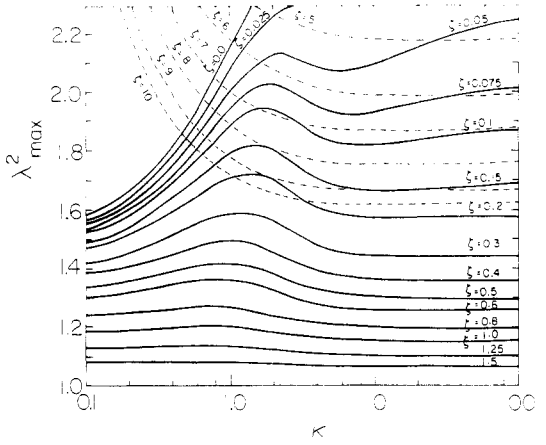

Figure 3. Position of the predicted maximum λ_{max}^2 as a function of κ for different ζ values in the Flory–Erman model.

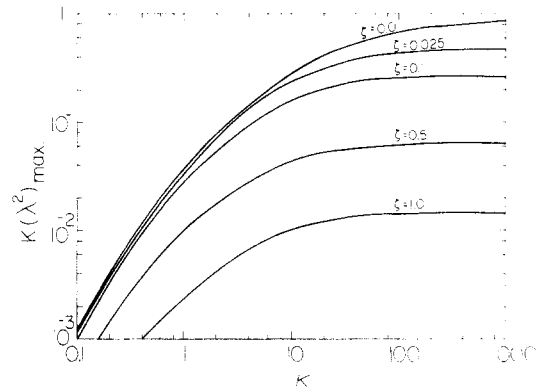

Figure 4. Highest value of $K(\lambda^2)$ in the Flory–Erman theory achievable for given κ and ζ values.

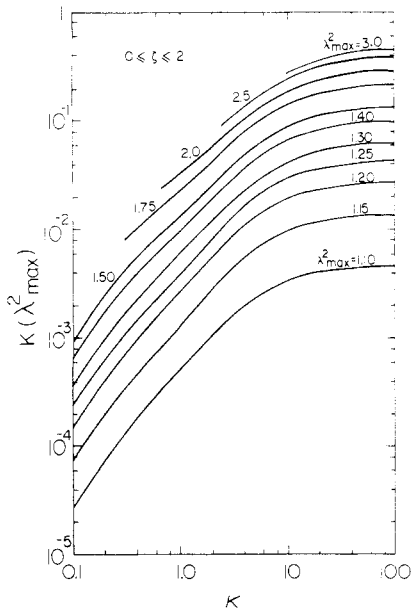

Figure 5. Value of $K(\lambda^2)$ at the maximum point as a function of κ for $0 \leq \zeta \leq 2$ in the Flory–Erman theory.

man), the broken line (Marrucci I–Gaylord), the dash–dot line (modified Graessley), and the dash–double dot line (Marrucci II) while the experimental curves are indicated by the solid line.

Marrucci I–Gaylord and Modified Graessley Models. The differences between curves of the Marrucci and Gaylord models and the modified Graessley model are negligibly small and well below experimental accuracy for all four sets of data. The agreement between theory and

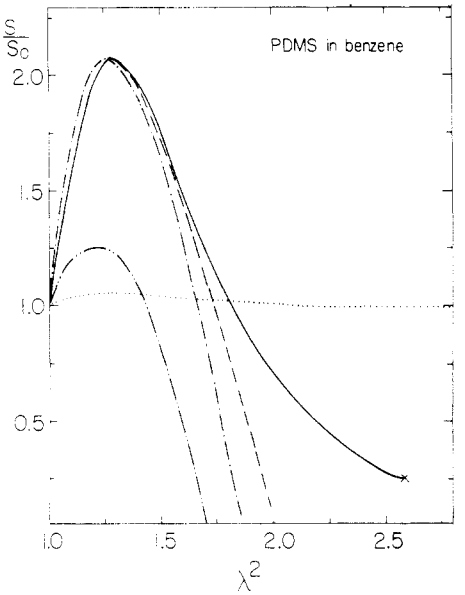

Figure 6. Reduced dilation modulus vs. λ^2 for PDMS swollen in benzene. Solid line, smoothed experimental data of Brotzman and Eichinger;[6] dashed line, Marrucci–Gaylord ($A = -0.338$, $B = 0.635$); dash–dot line, modified Graessley ($p = 0.119$, $\alpha = -0.988$); dotted line, Flory–Erman ($\kappa = 100$, $\xi = 0.57$); dash–double dot line, Marrucci II ($l_0/a_0 = -3.3$, $r = 0.65$). (×) indicates experimental saturation point.

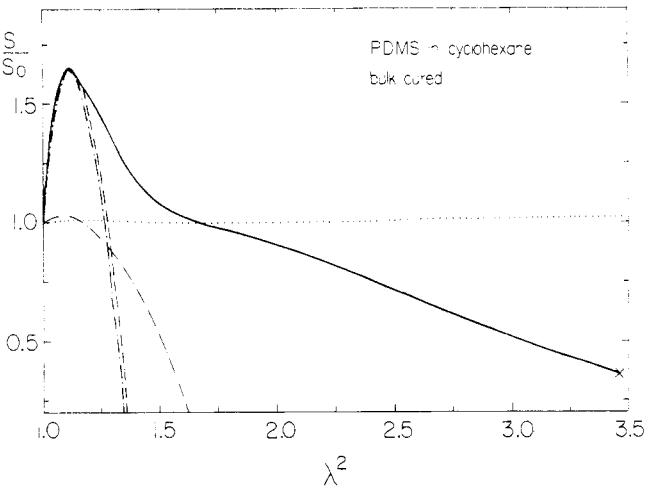

Figure 7. Reduced dilation modulus vs. λ^2 for bulk-cured PDMS swollen in cyclohexane. Solid line, smoothed experimental data of Brotzman and Eichinger;[6] other lines same as in Figure 6 with the following parameters: Marrucci–Gaylord, $A = -0.430$, $B = 0.560$; modified Graessley, $p = 0.115$, $\alpha = -1.0$; Flory–Erman, $\kappa = 100$, $\zeta = 1.15$; Marrucci II, $l_0/a_0 = -5.9$, $r = 0.41$.

experiment is good in the case of the PDMS–benzene system as shown in Figure 6. With the PDMS–cyclohexane system, for both the bulk- and solution-cured networks, shown in Figures 7 and 8, respectively, the agreement is good only over a portion of the dilation range. The theories are completely unable to describe the data for the natural rubber–benzene system, as can be seen in Figure 9. Looking at the parameter values listed in Table III, we find that for all of the data sets, the modified Graessley model was best fitted by using physically unrealistic parameters, namely, small negative values for the number of steps in a chain. Similarly, the Marrucci and Gaylord models require negative parameter values for the three PDMS systems and physically unacceptable positive values ($r \sim 2$, $a_0 \sim 10l_0$) for the natural rubber system.

Marrucci II Model. For only two out of the four systems tested here, a match was possible between the

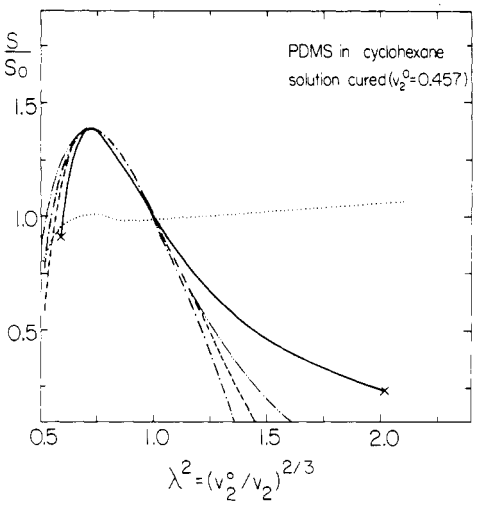

Figure 8. Reduced dilation modulus vs. λ^2 for solution-cured PDMS in cyclohexane. Solid line, smoothed experimental data of Brotzman and Eichringer;[5] (×) at left-hand side of solid line indicates dry network; (×) at right-hand of solid line shows saturation point. Other lines same as in Figure 6 with the following parameters: Marrucci–Gaylord, $A = -0.503$, $B = 0.362$; modified Graessley, $p = 0.094$, $\alpha = -0.992$; Flory–Erman, $\kappa = 1.9$, $\zeta = 2.7$; Marrucci II, $l_0/a_0 = 52.1$, $r = 0.0046$.

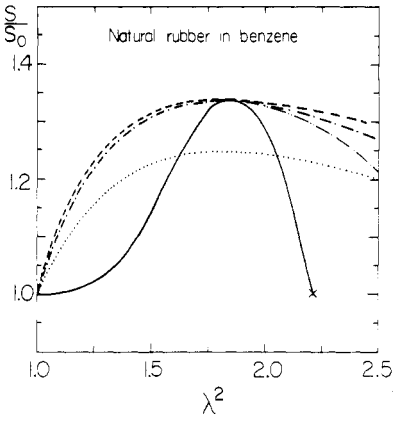

Figure 9. Reduced dilation modulus vs. λ^2 for natural rubber swollen in benzene. Solid line, smoothed experimental data of Gee, Herbert, and Roberts.[3] Other lines same as in Figure 6 with the following parameters: Marrucci–Gaylord, $A = -0.443$, $B = 0.905$; modified Graessley, $p = 0.117$, $\alpha = -0.804$; Flory–Erman, $\kappa = 100$, $\zeta = 0.115$; Marrucci II, $l_0/a_0 = -16.9$, $r = 0.39$.

experimental and predicted maxima. For the PDMS–benzene system (Figure 6) and PDMS–cyclohexane system (Figure 7) the highest maxima values obtainable by the model are indicated by the dash–double dot line. These are considerably below the experimental curve. A negative tube length to cross-sectional area ratio has been used to obtain these curves.

For the two remaining systems two sets of parameters have been obtained for each. In the case of the solution-cured PDMS–cyclohexane system one set of parameters involves negative l_0/a_0 and the other includes $r \cong 0$ (i.e., infinitely large tube diameter after curing). Only the latter set is depicted in Figure 8, demonstrating a marginal improvement over other models at the high-deformation part of the curve. The former set results in a curve that lies slightly below the Graessley model. For the natural rubber–benzene system the two curves obtained by the two parameter sets merge with the Graessley curve for $1.0 < \lambda^2 < 1.9$. For higher deformations one curve ($r = 0.40$, $l_0/a_0 = 10.8$) remains alongside the Graessley curve whereas the second curve ($r = 0.39$, $l_0/a_0 = -16.9$) declines slightly faster than the other models (cf. Figure 9) but still short of the decline exhibited by the experimental curve.

To summarize, the Marrucci II model evaluated by its ability to describe swelling data is inferior to the simpler Marrucci I model.

Flory–Erman Model. The curves for the Flory–Erman model in Figures 6–9 show very poor agreement with the data. Only for the natural rubber–benzene system can the magnitude of the peak be even approximately matched by theory, but at the expense of using an unrealistically large ζ value (8.35). The resulting curve is almost indistinguishable from the modified Graessley curve and for the sake of clarity is not depicted. A more reasonable ζ value, 0.115, yields a peak whose magnitude is considerably less than the observed magnitude, even for exceedingly large κ values.

An inspection of Figure 3 reveals that the location of the peaks in the PDMS–benzene system ($\lambda_{max}^2 = 1.27$) and PDMS–cyclohexane system ($\lambda_{max}^2 = 1.12$) determines the value of ζ unambiguously, independent of κ. Increasing the value of κ has the effect of increasing K to a point where a leveling off of the curve occurs, as shown in Figures 4 and 5. Even at these values, the highest attainable by the theory, the maxima are almost nonexistent when compared to the data in Figures 6 and 7. Finally, for the solution-cured system, the experimental maximum is located at $\lambda < 1$, which requires $\zeta > 2$. Here again, the magnitude of the peak is exceedingly small compared to the experimental peak. For similar systems in uniaxial deformation, Erman and Flory[15] used ζ values in the range 0–0.05; for PDMS swollen in benzene, 0.12 was used. These values are reasonable since ζ determines the degree of nonaffineness in the domain-of-constraint deformation. For this reason, one would intuitively expect relatively small values of ζ for the swelling experiments. Yet, as noted, large ζ values are needed here to obtain any given sort of compatibility with the data (the inability to match swelling data and uniaxial deformation data with comparable values of κ,ζ has also been pointed out recently by Brotzman and Eichinger[21]).

Conclusions

In this work we have tried to match the observed swelling behavior of polymer networks with the predictions of molecular theories. Only four of the nine models that were tested were able to give even a qualitative description of the experimentally observed phenomena. The modified Graessley primitive path model and the Gaylord and Marrucci tube models have a limited success in achieving quantitative agreement with the data, but only at the expense of using physically unrealistic parameter values. The treatment of chain size distribution as done in the Marrucci II model has a negative effect on the ability of this model to describe the data, possibly due to its failure to account for junction contribution to the network free energy. The Flory–Erman constrained junction fluctuation theory is very far from quantitatively describing swelling behavior, contrary to a statement to this effect by Brotzman and Eichinger.[6]

The inability of *all* of the existing molecular theories to satisfactorily describe swelling behavior may be a result of the inadequacy of these theories at their present level of development. However, it is quite possible that the fault resides in the Flory–Rehner assumption of free energy separability. The observed dependence of the reduced dilation modulus on the nature of solvent[6,21] contrary to the Flory–Rehner theory adds weight to this possibility. The implications of this assessment for the conventional method of determining cross-linking density should be kept in mind.[3]

In the next paper in this series, we will test the multiaxial deformation predictions of various molecular theories of rubber elasticity.

Acknowledgment. We are indebted to Prof. W. W. Graessley and Prof. L. R. G. Treloar for their valuable comments.

Appendix A. Calculation of $S(\lambda)$

Following Flory and Rehner[2] we assume that the change in free energy ΔA due to the mixing of a pure solvent (species 1) with a cross-linked polymer is given by the additive contribution of the free energy of mixing ΔA_M and the elastic free energy ΔA_{el}. We further assume that the free energy of mixing for a given solvent–polymer pair is identical regardless of whether the polymer is cross-linked or not. (For further discussion of this point, cf. Brotzman and Eichinger[6]).

The chemical activity of the solvent in a swollen gel is given by

$$\ln a_{1,c} = (kT)^{-1}(\partial\Delta A/\partial n_1)_{T,P} = (kT)^{-1}(\partial\Delta A_M/\partial n_1)_{T,P} + (kT)^{-1}(\partial\Delta A_{el}/\partial n_1)_{T,P} \quad \text{(A1)}$$

where n_1 is the number of moles of solvent in the system. Similarly, the solvent activity in a solution of the uncross-linked polymer is

$$\ln a_{1,u} = (kT)^{-1}(\partial\Delta A_M/\partial n_1)_{T,P} \quad \text{(A2)}$$

The dilation modulus is defined as

$$S = \lambda \ln (a_{1,c}/a_{1,u}) = \lambda(kT)^{-1}(\partial\Delta A_{el}/\partial n_1)_{T,P} \quad \text{(A3)}$$

The derivative in eq A3 can be evaluated by

$$\left(\frac{\partial\Delta A_{el}}{\partial n_1}\right)_{T,P} = \left(\frac{\partial\Delta A_{el}}{\partial\lambda}\right)_{T,P}\left(\frac{\partial\lambda}{\partial n_1}\right)_{T,P} \quad \text{(A4)}$$

For isotropic swelling the deformation ratio λ is given by

$$\lambda = \left(\frac{V}{V_0}\right)^{1/3} = \left(\frac{V_d + n_1\tilde{v}_1}{V_0}\right)^{1/3} = \left(v_2^0 + \frac{n_1\tilde{v}_1}{V_0}\right)^{1/3} \quad \text{(A5)}$$

Here, $\tilde{v}_1$ is the molar volume of the solvent and v_2^0 is the polymer volume fraction when the cross-linking took place. V, V_d, and V_0 are the total volume of the swollen network, the volume of the dry network, and the volume of the network in the curing stage, respectively. For network formed in bulk, $V_d = V_0$. When eq A5 is used in (A4) and (A3), we obtain

$$S = \frac{(\tilde{v}_1/V_0)}{3\lambda kT}\left(\frac{\partial\Delta A_{el}}{\partial\lambda}\right)_{T,P} \quad \text{(A6)}$$

References and Notes

(1) Gottlieb, M.; Gaylord, R. J. *Polymer* **1983**, *24*, 1644.
(2) Flory, P. J.; Rehner, J., Jr. *J. Chem. Phys.* **1943**, *11*, 521; **1950**, *18*, 108; **1950**, *18*, 112.
(3) Gee, G.; Herbert, J. B. M.; Roberts, R. C. *Polymer* **1965**, *6*, 541.
(4) Yen, L. Y.; Eichinger, B. E. *J. Polym. Sci., Polym. Phys. Ed.* **1978**, *16*, 121.
(5) Brotzman, R. W.; Eichinger, B. E. *Macromolecules* **1981**, *14*, 1445.
(6) Brotzman, R. W.; Eichinger, B. E. *Macromolecules* **1982**, *15*, 531.
(7) Marrucci, G. *Rheol. Acta* **1979**, *18*, 193. Graessley, W. W. *Polym. Prepr., Am. Chem. Soc., Div. Polym. Chem.* **1981**, *22* (2), 152.
(8) Ball, R. C.; Doi, M.; Edwards, S. F.; Warner, M. *Polymer* **1981**, *22*, 1010.
(9) Flory, P. J. *J. Chem. Phys.* **1950**, *18*, 108; "Principles of Polymer Chemistry", Cornell University Press: Ithaca, NY, 1953.
(10) James, H. M. *J. Chem. Phys.* **1947**, *15*, 651. James, H. M.; Guth, E. *Ibid.* **1947**, *15*, 669. Duiser, J. A.; Staverman, A. J. "Physics of Non-Crystalline Solids"; Prins, J. A., Ed.; North-Holland Publishing Co.: Amsterdam, 1965; p 376. Gaylord, R. J. Ph.D. Thesis, SUNY at Syracuse, 1973. Smith, K. J., Jr.; Gaylord, R. J. *J. Polym. Sci., Polym. Phys. Ed.* **1975**, *13*, 2069. Graessley, W. W. *Macromolecules* **1975**, *8*, 865. Flory, P. J. *Proc. R. Soc. London, Ser. A* **1976**, *351*, 351.
(11) Ronca, G.; Allegra, G. *J. Chem. Phys.* **1975**, *63*, 4990.
(12) Flory, P. J. *J. Chem. Phys.* **1977**, *66*, 5720. Erman, B.; Flory, P. J. *Ibid.* **1978**, *68*, 5363. Flory, P. J. *Macromolecules* **1979**, *12*, 119. Flory, P. J.; Erman, B. *Ibid.* **1982**, 15, 800.
(13) Graessley, W. W. *Adv. Polym. Sci.* **1982**, *46*, 67.
(14) Edwards, S. F. *Br. Polym. J.* **1977**, *9*, 140.
(15) Edwards, S. F. *Proc. Phys. Soc.* **1967**, *92*, 9.
(16) DiMarzio, E. A. *Polym. Prepr., Am. Chem. Soc., Div. Polym. Chem.* **1968**, *9* (1), 256.
(17) de Gennes, P.-G. *J. Phys. (Paris), Lett.* **1974**, *35*, L-133.
(18) Marrucci, G. *Macromolecules*, **1981**, *14*, 434.
(19) Gaylord, R. J. *Poly. Eng. Sci.* **1979**, *19*, 263; *Polym. Bull.* **1982**, *8*, 325; **1983**, *9*, 181.
(20) Erman, B.; Flory, P. J. *Macromolecules* **1982**, *15*, 806.
(21) Brotzman, R. W.; Eichinger, B. E. *Macromolecules* **1983**, *16*, 1131.